

**DISTRIBUTION OF THE REMAINING TRITIUM IN THE LHD VACUUM VESSEL**

S. Masuzaki

National Institute for Fusion Science

Toki 509-5292, Japan

The Graduate University for Advanced Studies

SOKENDAI, Toki 509-5292, Japan

E-mail: masuzaki.suguru@nifs.ac.jp

M. Yajima<sup>1,2</sup>, M.Z. Zhao<sup>1</sup>, K. Ogawa<sup>1,2</sup>, M. Isobe<sup>1,2</sup>, M. Tanaka<sup>1,2</sup>, M. Tokitani<sup>1,2</sup>, G. Motojima<sup>1,2</sup>, N Yoshida<sup>3</sup>, S.E. Lee<sup>4</sup>, Y. Hatano<sup>4</sup>, Y. Torikai<sup>5</sup>, N. Ashikawa<sup>1,2</sup>, Y. Nobuta<sup>6</sup>, Y. Oya<sup>7</sup>, T. Otsuka<sup>8</sup><sup>1</sup> National Institute for Fusion Science, Toki 509-5292, Japan<sup>2</sup> The Graduate University for Advanced Studies, SOKENDAI, Toki 509-5292, Japan<sup>3</sup> Kyushu University, Kasuga 816-8580, Japan<sup>4</sup> University of Toyama, Toyama 930-8555, Japan<sup>5</sup> Hokkaido University, Sapporo 060-0808, Japan<sup>6</sup> Ibaraki University, Mito 310-8512, Japan<sup>7</sup> Shizuoka University, Shizuoka 422-8529, Japan<sup>8</sup> Kindai University, Higashi-Osaka 577-8502, Japan**Abstract**

In the Large Helical Device (LHD), deuterium plasma experiment has been conducted since 2017. This is the first opportunity in stellarator / heliotron devices to reveal the transport of tritium generated by deuterium-deuterium fusion reactions not only in core plasma but also outside plasma. Dedicated analyses of the remaining tritium in the LHD vacuum vessel have been conducted, and results of the analyses suggest that tritium remains densely in divertor tiles and sparsely in the first wall. Furthermore, an asymmetry was observed in remaining amounts of tritium in divertor tiles located at symmetric positions. This asymmetric distribution is consistent with the distribution of lost points of energetic triton on plasma facing surfaces calculated by a Lorentz orbit following code, LORBIT. A depth profile of remaining tritium in a baffle part of an inner divertor tile, on which no divertor plasma irradiation, shows weakly peaked profile in which the peak locates approximately 4 - 6  $\mu\text{m}$  from the surface, which is much deeper than the penetration length of thermalized tritium. These results suggest the origin of the remaining tritium in divertor tiles is mainly energetic triton.

**1. INTRODUCTION**

Deuterium plasma experiment has been started in LHD since 2017 [1]. This is the first opportunity of triton/tritium related studies in stellarator/heliotron devices which have three-dimensional magnetic configurations and vacuum vessel structures. Analyses of remaining tritium in plasma facing components are important from viewpoints of the studies of triton transport from generation to loss on plasma facing surfaces, tritium migration, and safety of in-vessel works. In tokamaks, such analyses have been conducted [2-7]. It was revealed that the distribution of lost points of energetic triton on plasma facing components affects the distribution of remaining tritium in the case of deuterium plasma experiment.

During the first deuterium plasma experiment in LHD, the amount of generated tritium was estimated from the data of neutron monitors [8], and that was approximately 6.4 GBq ( $\sim 3.6 \times 10^{18}$  T) [9]. A part of generated tritium was removed from the vacuum vessel by pumping systems. The exhaust gas lines from all vacuum pumping systems are integrated and connected to the exhaust detritiation system for tritium removal, and the tritium monitoring system is installed at the inlet of the exhaust detritiation system [9]. The tritium monitoring system consists of the water bubbler system for the measurement of total tritium amount using the liquid scintillation counter. The total amount of exhausted tritium was 32.8% of generated tritium at the end of the hydrogen plasma experimental campaign following the first deuterium plasma experimental campaign. The exhausted rate of tritium is little bit larger than that in JT-60 and JET [9]. This result means that more than 60 % of generated tritium in the first deuterium plasma experiment remained in the vacuum vessel before the second deuterium plasma experiment.

Analyses of remaining tritium in plasma facing components after the first deuterium plasma experiment have been conducted in LHD. The analysis using the tritium imaging plate technique [6] has been revealed the two-dimensional profiles of remaining tritium on surfaces of divertor tiles and first wall panels [10], the thermal desorption method [11], hydrothermal treatment [12-14], and the full combustion method [15] have been utilized

for the analysis of remaining tritium amount in material probes made of stainless-steel and divertor tiles made of graphite.

In this presentation, the obtained data in previous analyses are summarized, and some new data are added to reveal the distribution of remaining tritium in the LHD vacuum vessel after the first deuterium plasma experiment. The result of tracing of energetic triton generated in core plasma also shown to compare the distribution of lost points of energetic triton on plasma facing surfaces to the distribution of remaining tritium. In the next section, plasma facing components in the LHD vacuum vessel are mentioned, and the tracing of energetic triton and the result of the tracing is mentioned in the third section. In the fourth section, experimental setup such as positions of material probes and analyzed divertor tiles, methods for the analysis of remaining tritium in materials are mentioned. Results of analyses are shown and discussed in the fifth section, and this study summarized in the last section.

## 2. PLASMA FACING COMPONENTS IN LHD

In LHD, for the three-dimensionality of the magnetic configuration produced by a pair of helical coils as shown in Fig. 1(a), the structure of the vacuum vessel is also three-dimensional. Figure 1(b) shows a photo of inside the vacuum vessel. The vacuum vessel wall including helical coil cans is covered by first wall panels made of the stainless-steel type 316L (hereafter SUS316L) which is cooled by water. The heliotron-type magnetic configuration is equipped with an intrinsic divertor magnetic structure so called helical divertor between helical coil cans, and divertor components such as divertor tiles and dome are there as shown in Fig. 1(b) and (c). Divertor tiles and dome are made of isotropic graphite, and they are cooled by water [15]. The plasma facing surface area of the first wall and divertor tiles are approximately 400 m<sup>2</sup> without including the surface in ports and approximately 46 m<sup>2</sup>, respectively.

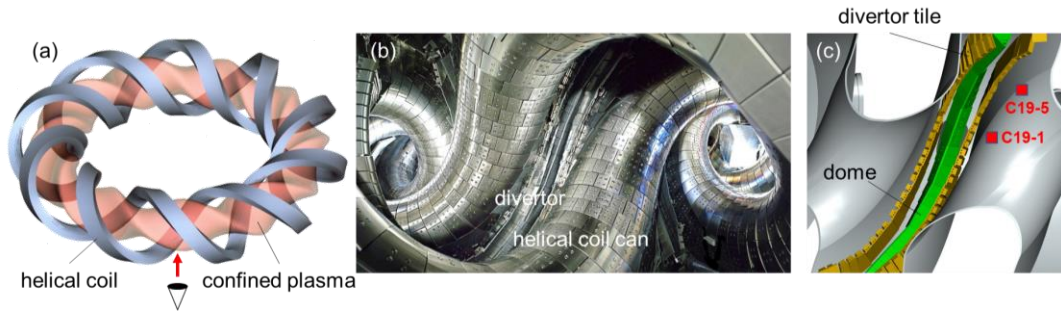


Fig. 1 (a) Helical coils and confined plasma, (b) and (c) are a photo of inside the vacuum vessel and an inner divertor region from the eye shown in (a), respectively. Red squares in (c) show positions of material probes mentioned in the section 4.2.

## 3. DISTRIBUTION OF ENERGETIC TRITON ON THE PLASMA FACING COMPONENTS

### 3.1. Tracing of energetic triton

Tracing of energetic triton generated by deuterium-deuterium fusion reactions has been carried out by using a Lorentz orbit following code, LORBIT [16] with taking into account plasma facing components such as divertor tiles and dome. In this study, a typical experimental condition in which plasma is heated by neutral beams in the standard magnetic configuration (major radius of the magnetic axis,  $R_{ax} = 3.6$  m, toroidal field strength,  $B_t = 2.75$  T, direction of  $B_t$  is counter-clockwise (CCW)), and line-averaged electron density, electron and ion temperature were  $2 \times 10^{19} /m^3$ , and 3 keV, respectively, was considered. The distribution of points of triton generation was calculated by using FIT3D-DD code [17]. Promptly lost triton without collision with background plasma particle were considered in this study. The result of the tracing shows that approximately 40 % of generated triton are promptly lost on plasma facing surfaces [16].

### 3.2. Distribution of lost points of energetic triton

Figure 2(a) shows the top view of four divertor tile arrays in the helical divertor in a half part of LHD. Green dots in the figure are lost positions of high energy triton calculated by using LORBIT code for the standard operational magnetic configuration with the CCW  $B_t$ . It is clearly shown in Fig. 2(a) that high energy tritons are lost to divertor region asymmetrically. In this case, the lost positions are only at red colored tile arrays.  $\mathbf{B} \times \text{grad } \mathbf{B}$  drift dominates the orbit loss of energetic triton, and thus the asymmetry depends on the  $B_t$  direction. In Fig. 2(b), red dots show lost points of energetic triton in a top part of an inner divertor. Lost points are mainly on divertor tiles but also on

dome and the first wall beside divertor tiles. Approximately 72 % of lost points are on divertor tiles, 7 % is on dome tiles, and 21 % is on the first wall.

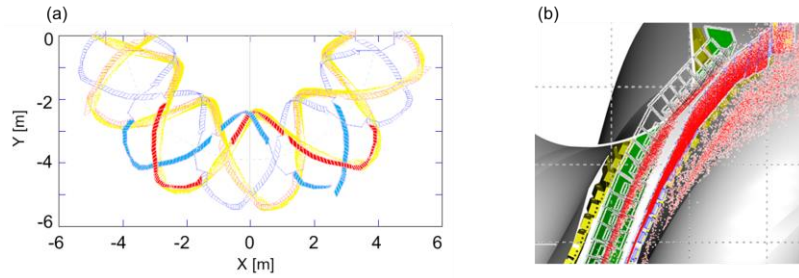


Fig. 2. (a) Top view of the four divertor tile arrays in LHD, which are shown by blue and red lines. The hatched parts of two arrays are corresponding to L and R arrays in Fig. 3(a). Yellow dots are lost points of energetic triton on plasma facing components such as divertor tiles, dome and the first wall calculated by using the LORBIT code in the standard magnetic configuration with the CCW Bt. All lost positions of triton are on the red tiles array side in this condition. (b) Lost points on a top part of an inner divertor which is a magnified figure of Fig. 1(c). Red dots are lost points.

## 4. EXPERIMENTAL SETUP

### 4.1. Analyzed divertor tiles

After the first deuterium plasma experiment, 20 divertor tiles shown in Fig. 3(a) were retrieved from the vacuum vessel for tritium analyses. In the figure, “I-“ and “O-“ mean “inner” and “outer”, and “L” and “R” mean “left” and “right”. Divertor tiles with same number such as “I-1L” and “I-1R” were located at the symmetric positions. Figures 3(b) and (c) show an inner and an outer divertor tile, respectively. An inner divertor tile consists of two graphite parts, ‘baffle part’ and “divertor trace part”, which are cooled by a water-cooling pipe placed between the two parts. Typical sizes of an inner and an outer divertor tiles are  $0.1 \text{ m} \times 0.3 \text{ m}$  ( $0.15 \text{ m} + 0.15 \text{ m}$ )  $\times 0.06 \text{ m}$  and  $0.09 \text{ m} \times 0.2 \text{ m} \times 0.015 \text{ m}$ , respectively. In the case of an inner divertor tile, the strike-point is on the “divertor trace part”, and the “baffle part” is not irradiated plasma. As the result, as shown in the photo in Fig. 3(b), trace of the strike-point is only on the divertor trace part, and erosion and deposition are significant on the divertor trace part.

The result of the orbit tracing of energetic triton shows that number of lost triton on inner divertor tiles are approximately five times larger than that on outer divertor tiles. Five inner divertor tiles, I-1R, I-3R, I-6R, O-3L and O-6L were cut into small pieces for a quantitative analysis of amount of remaining tritium using the full combustion method, and depth profile analysis of remaining tritium using the combination method of sputtering treatment and the imaging plate technique. The analyses methods and results are mentioned in the next section.

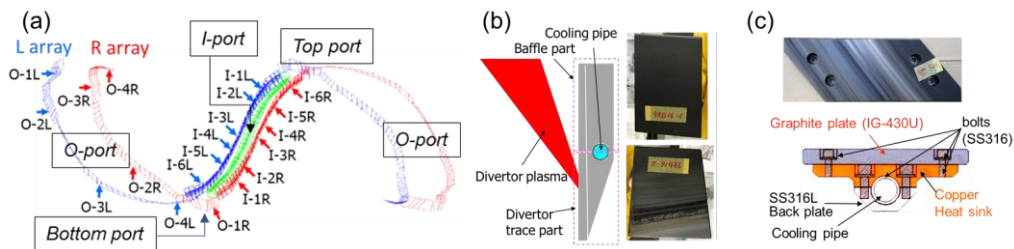


Fig. 3. (a) Two divertor tiles arrays which are hatched by blue and red in Fig. 3 (a). Positions of analyzed divertor tiles are shown. “I-“ and “O-“ mean inner and outer, respectively, and “L” and “R” mean left and right, respectively. Analyzed inner and outer divertor tiles were retrieved from toroidal section #9 and #7, respectively [10]. (b) A side view and a photo of an inner divertor tile. An inner divertor tile consists of two graphite parts, ‘baffle part’ and “divertor trace part”, which are cooled by a water-cooling pipe placed between the two parts. (c) A side view and a photo of an outer divertor tile. An outer divertor tile consists of a graphite tile and a water-cooled copper heat sink.

### 4.2. Material probes

For the three-dimensionalities of the magnetic configuration, particle and heat loads on divertor tiles, and the vacuum vessel structure, mechanisms of formation of deposition-dominant and erosion-dominant areas are more complicated than that in axisymmetric devices such as tokamaks. Material migration in the vacuum vessel has been investigated by using material probes in LHD since the first experimental campaign [18]. Results of previous

material probes analyses and the colorimetric analysis of the surface of the first wall [19], positions of material probes for the first deuterium plasma experiment were decided. Stainless-steel plates (type-316L) were used as material probes. A typical size of the probe was 8 mm × 10 mm with thickness of 0.2 mm. They were installed on the first wall panels as shown in Fig. 1(c) and Fig. 4. Fig. 4(a) shows positions of material probes in a cross-sectional view at the equator of a half part of the vacuum vessel. There were three groups of material probes as below: (1) below each outer horizontal port (O-port) shown by blue squares, (2) on helical coil can at each toroidal section shown by green squares, and (3) other positions in the toroidal section #9 shown by red squares. Positions of material probes of (1) and (2) in a poloidal cross-section are shown in Fig. 4(b). Probes in the toroidal section #9, positions of C19-1 and 5 were on the helical coil can near the equator at the inboard-side as shown in Fig. 1(c), and C19-6 was installed on the bottom private region as shown in Fig. 4(a). Probes C19-2 to 4 were installed on the helical coil can near the equator at the outboard side as shown in Fig. 3(a). Probes C19-3 and 4 are in the deposition-dominant area, and the other probes positions are in the erosion-dominant area.

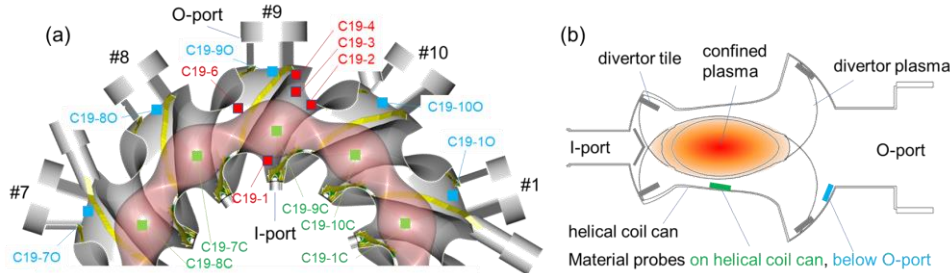


Fig. 4. (a) Cut view of the vacuum vessel at the equator. Positions of material probes in a half part of the vacuum vessel are shown. Blue and green squares are positions of material probes installed below O-ports (C19- (toroidal section number) O) and on coil cans (C19- (toroidal section number) C), respectively. Red squares are positions of material probes located various positions in the toroidal section of #9 (C19- number). In the names of material probes, “C19” means the LHD 19<sup>th</sup> experimental campaign. (b) Schematic view of positions of material probes on helical coil can (green) and below O-port (blue) in a horizontally elongated cross-section.

## 5. METHODS OF ANALYSES AND RESULTS

### 5.1. Tritium imaging plate technique (TIPT) [10]

The tritium imaging plate (IP) technique has been used in tokamaks to investigate distributions of remaining tritium on plasma facing components [2, 5, 6]. The tritium distribution near surface is shown as the distribution of photo-stimulated luminescence (PSL) intensity, which can be considered proportional to tritium amount within the escape depth of  $\beta$ -rays from tritium decay. The imaging plate used in this study was BAS IP TR2040 (GE Healthcare Japan) which has high sensitivity for low energy  $\beta$ -rays from tritium decay (up to 18.6 keV). The surface of the IP was in contact with the surfaces of analysed divertor tiles and material probes in a dark room. Typical times for the IP exposure were 24 hours for divertor tiles and 72 hours or more for material probes. In the measurement, between objects measured and the IP, a polyphenylene sulphide (PPS) film with 1.2  $\mu\text{m}$  of thickness through which  $\beta$ -rays can reach the IP was inserted to avoid contamination of the IP with tritium. In the case of material probes, the effects of radiation sources other than tritium such as  $^{58}\text{Co}$  generated in a neutron irradiated stainless-steel and  $\beta$ -rays induced X-rays must be considered. Therefore, the measurement with 12  $\mu\text{m}$  thick PPS film which prevents  $\beta$ -rays from tritium decay to reach the IP was also conducted for material probes. After each exposure, the IP was processed by using an imaging plate reader (BAS2500, FUJIFILM) to obtain a digitized image with a spatial resolution of 50  $\mu\text{m}$ . For the low energy of  $\beta$ -rays from tritium decay, the tritium detection by TIPT is limited by the escape depth of  $\beta$ -rays which depends on densities of materials in which the tritium remained. In the case of carbon and iron, the depth is approximately 1  $\mu\text{m}$  and a few hundred nm, respectively.  $\beta$ -rays from remaining tritium deeper than the escape depths cannot be detected by TIPT.

Figure 5(a) shows examples of images of tritium distributions on divertor tiles, I-3L and I-3R, which located at symmetric positions near the equatorial plane as shown in Fig. 4(a). Remaining tritium in baffle parts is larger than that in divertor trace parts of both tiles. Asymmetry of remaining tritium in baffle parts is observed. On divertor trace parts, less remaining tritium is observed at divertor trace area than other area. Fig. 5(b) – (d) show surface area and exposure time averaged PSL intensities on divertor tiles are shown. In each figure, upper and lower panels show cases of blue and red colored divertor tiles arrays in Fig. 4(a). The asymmetry of remaining tritium is clearly observed on baffle part tiles. For divertor trace part tiles and outer divertor tiles, the asymmetry is also observed although the degrees of the asymmetry of these tiles are less than those of baffle part tiles.



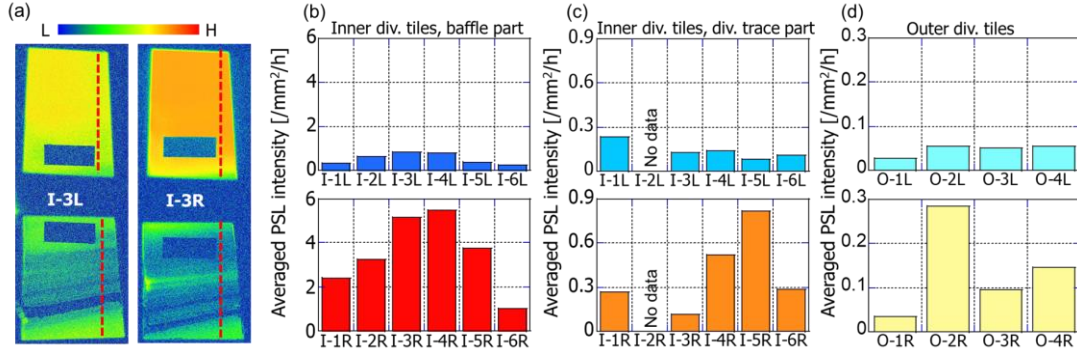


Fig. 5. (a) Images of tritium distributions on divertor tiles, I-3L and I-3R, obtained by the TIPT. Upper and lower parts are the baffle part and the divertor trace part. There were labels at rectangular areas on all tiles (see Fig. 4(b)), and that is why PSL intensities there is low. Averaged IP intensity (PSL intensity) on surfaces of (b) inner divertor tiles (baffle part), (c) inner divertor tiles (divertor trace part), and (d) outer divertor tiles. The data shown in this figure are the same data as presented in [10]

Figure 6 shows results of the IP measurement for material probes located on the first wall. The averaged PSL intensities of material probes are much less than those of divertor tiles except C19-3 and 4 which were located at deposition-dominant area. For some probes, amounts of remaining tritium were below the detection limit under the measurement condition in this study. Deposition layers on C19-3 and 4 were observed by a transmission electron microscope (TEM) and an energy dispersive X-ray analysis (EDX), and their thickness were several hundred nm and approximately 2  $\mu m$ , respectively, and their dominant element was carbon [11]. The PSL intensities of C19-5 and C19-9O are relatively large. On C19-9O, relatively thick deposition layer in which boron was the dominant element was observed by TEM and EDX. On the other hand, C19-5 was located at erosion-dominant area, and deposition layer was not observed by TEM.

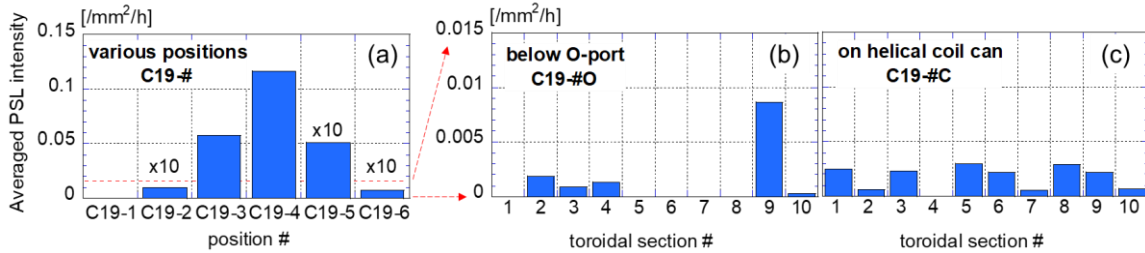


Fig. 6. Averaged PSL intensities on material probes located (a) at various positions, (b) below O-ports, and (c) on helical coil cans from the left. In the various positions case, the intensities of C19-2, 5 and 6 are multiplied by 10.

## 5.2. Measurements of remaining tritium content in divertor tiles and material probes

To measure remaining tritium contents in divertor tiles and material probes, a thermal desorption with a moist air was conducted [11, 15]. In the case of divertor tile samples, this method is so called full combustion method. Fig. 7 shows the scheme of this method. A quartz tube with inner diameter of 16 mm, and 300 mm long surrounded by an electric heater was utilized as a reactor. A thermocouple touched the outside of the tube to monitor the temperature of a sample in the tube. From the upstream of the reactor, moist air flew into the reactor with the flow rate of 300 SCCM, and then, air including tritium flew into an oxidation reactor with two palladium catalysts as shown in Fig. 7. The catalyst is supported on a metal honeycomb [20], and was heated by a heater to 668 K to oxidize tritium in chemical forms of tritiated hydrogen gas and tritiated hydrocarbons into tritiated water vapor. The tritiated water was collected by water bubblers, in which 15 ml of pure water was contained. At each bubbler, the tritiated water was collected with the collection rate of more than 99%. A sample placed on an alumina boat was inserted into the tube, and was heated up to 1183 K with taking approximately 30 min. The temperature was

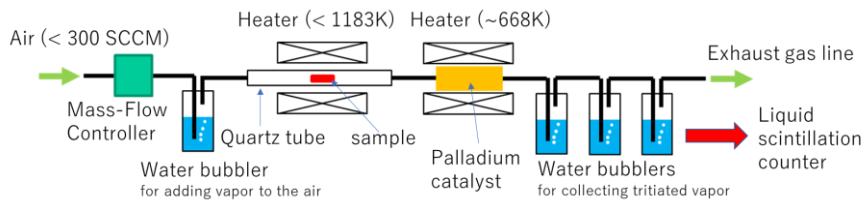


Fig. 7. A scheme of the thermal desorption (combustion) method

kept for 10 min. to 30 min. to maintain combustion of a sample, and then, the heater was turned off. From each bubbler, 10 ml of water was sampled, and was mixed with 10 ml of liquid scintillator in a polyethylene vial, and the tritium activity was determined by a liquid scintillation counter.

Remaining tritium in the five divertor tiles, I-3L, 6L, 1R, 3R, 6R, were analyzed by using the combustion method. They must be cut into small pieces for the size limit of the quartz tube. In the case of I-3L and 3R, they were cut along the red dashed lines in Fig. 5(a), and other tiles were also cut in the same manner. Typical size of a small piece was 15 – 25 mm × 5 mm with thickness of 1 mm. Results of the analysis with the full combustion method are shown in Fig. 8(a). As observed by the analysis using TIPT, a large asymmetry of remaining tritium between the “L” and “R” tiles. Figure 8(b) shows number of lost points of energetic triton on the three divertor tiles, I-1R, 3R, and 6R. Figure 8(a) and (b) shows qualitative agreement between the ratio of measured amounts of remaining tritium in the three tiles and the ratio of calculated numbers of lost points of energetic triton on them.

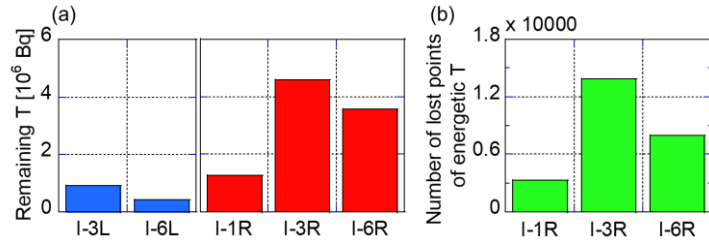


Fig. 8. (a) Evaluated total remaining amount of tritium in five inner divertor tiles. (b) Number of lost points of energetic triton on three inner divertor tiles calculated by using the LORBIT code.

Figure 9 shows the results of the measurement of remaining tritium in material probes by using the thermal desorption method. In the case of various positions probes, Fig.9(a) and Fig. 6(a) show the same result, that is, relatively large amounts of tritium remained in C19-3 and 4. The amounts of remaining tritium in C19-5 and C19-9O are relatively large as the same as the result of TIPT.

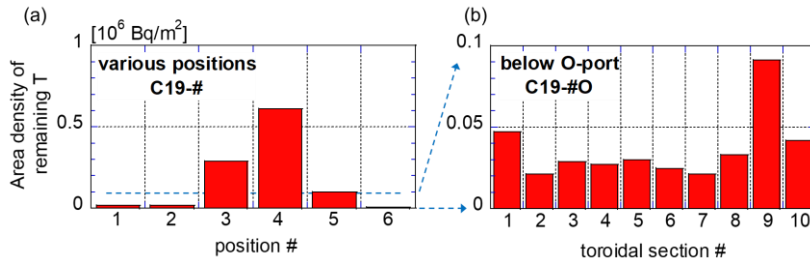


Fig. 9. Area density of remaining tritium on material probes located at (a) various positions and (b) below O-ports. The data shown in (a) is the same as in [11]

The hydrothermal treatment using an autoclave vessel (SAN-AI Science Co. Ltd.) [12] was applied to measure remaining content of tritium in material probes on helical coil cans, C19-1C to 10C [13]. The results show that amounts remaining tritium in these probes are similar to those in the probes below O-port shown in Fig. 9(b).

### 5.3. Measurement of a depth profile of remaining tritium in a divertor tile

Depth profile of remaining tritium is an important data to reveal the origin of the remaining tritium. For the graphite case, if the origin is thermalized triton, the penetration depth of triton is much shallower than 1  $\mu$ m. However, if the origin is energetic triton with kinetic energy of 1 MeV, its penetration depth is approximately 8  $\mu$ m for the case of normal incidence. To investigate the depth profile of remaining tritium in the baffle part of the I-3R divertor tile, a combination analysis using the IP technique and a sputtering treatment was conducted [15]. For the sputtering treatment, a glow discharge optical emission spectroscopy [21] device (GDA750, Rigaku) was utilized. In the device, a surface of a sample works as a cathode of a RF-glow discharge. The diameter of the plasma column in the glow discharge was 4 mm in this study. A sample surface was sputtered by argon ion bombardments. Five samples cut from the tile were treated with different discharge times from 100 s to 1000 s. After the treatment, a crater was formed by erosion with sputtering. Depths of craters were measured by using a profilometer with a stylus. Then the IP technique was applied to the five treated samples. Figure 10(a) shows the result of the combination analysis. The vertical axis shows PSL intensities in craters normalized by PSL intensities on original surface. It is clearly shown that the peak position of the depth profile is around 4 - 6  $\mu$ m from the surface. The profile weakly decreases toward the surface, and steeply decreases to deeper region.

To obtain information of remaining tritium in deeper region in divertor tiles than the escape depth of  $\beta$ -rays from tritium decay, measurement of bremsstrahlung and characteristic X-rays induced by  $\beta$ -rays from tritium decay ( $\beta$ -ray induced X-ray spectrometry, BIXS) was also conducted for the same tile as the combination analysis mentioned above [22]. Obtained X-rays spectrum was compared with the simulation using Geant4 code [23] with assuming the penetration depth of tritium is 1, 4, 6, and 8  $\mu\text{m}$ , and tritium density is assumed to be same up to the penetration depth, and zero in deeper region. Figure 10(b) shows the result of the simulation for the case of the penetration length of 6  $\mu\text{m}$ . Among these assumed penetration depths, the 6  $\mu\text{m}$  case is the best.

From these results of the combination analysis and BIXS, it can be concluded that the origin of remaining tritium in the baffle part is energetic triton.

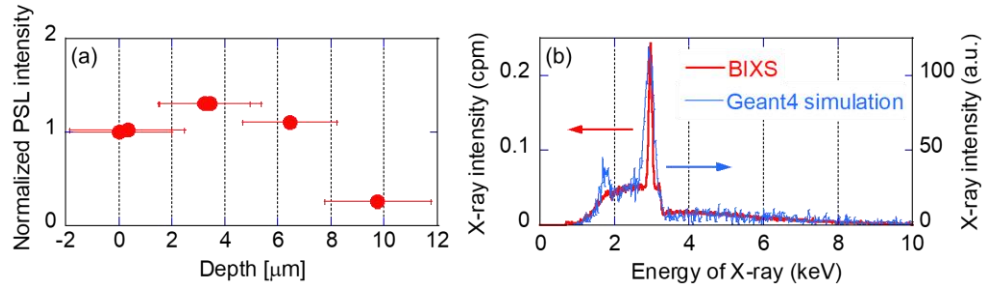


Fig. 10. (a) Depth profile of remaining tritium shown by the normalized PSL intensity in the baffle part of the I-3R tile. The definition of the normalized by the PSL intensity is explained in the text. (b) X-ray spectra from the baffle part of the I-3R tile. Black and red curves show the measured spectrum by BIXS and simulated using Geant4 by assuming penetration depth of tritium is 6  $\mu\text{m}$  [22]. The data in (a) is the same data shown in [15].

## 6. DISCUSSION

In this section, causes of the asymmetry in the remaining tritium distribution, and the mechanism of tritium retention in the first wall are discussed from the data shown in above sections.

Results of TIPT and the thermal desorption/full combustion method clearly show that tritium remaining in divertor tiles densely and sparsely in the first wall. For divertor tiles, the observed asymmetric distribution of remaining tritium is mainly caused by the asymmetric loss of energetic triton. As shown in Fig. 2, lost points of energetic triton are only on the red colored divertor side in Fig. 2 and Fig. 3 in the case of CCW  $B_t$  direction which is the standard direction in LHD experiment. In the case of the first deuterium plasma experiment, approximately 91 % of triton were generated by deuterium – deuterium fusion reactions under the condition of the CCW  $B_t$ , and thus the clear asymmetry appears. Up to here, the case of promptly lost energetic triton has been discussed. The amount of promptly lost triton was investigated by using the LORBIT code, and it was revealed that approximately 40 % of generated triton is lost promptly [16]. Other generated triton collide with neutral beam and/or background plasma particles, and they lose their kinetic energy. So far, results of a calculation of lost points on plasma facing surfaces for triton after collisions has not been conducted but the calculation for proton with kinetic energy of 180 keV which is the acceleration energy of neutral beam injectors was conducted [24]. In that case, the lost points distribution depends on the direction of  $B_t$  as the same as the case of energetic triton in relatively low  $\beta$  plasma case.

In the case of divertor trace part tiles and outer divertor tiles, the amounts of remaining tritium are smaller than those in baffle tiles, and the asymmetry is weaker than that in the baffle tiles case. The calculation using the LORBIT shows that the number of lost points on divertor trace part tiles and outer divertor are generally smaller than that on baffle tiles [15]. Furthermore, strike points of divertor plasma are on divertor trace part and outer divertor tiles as shown photos in Fig. 3, and remained tritium in the tiles can be released with divertor plasma irradiation especially during the hydrogen plasma experiment after the deuterium plasma experiment. In the hydrogen plasma experiment, approximately 64 % of experiments were conducted in the CCW  $B_t$  condition. It was revealed that the asymmetry appears not only for high energy particle but also thermalized ions [25]. As the result, the asymmetry in the remaining tritium can be weaker.

For the case of the first wall, only 21 % of lost points of energetic triton is observed near divertor tiles as mentioned in the section 3.2. As the result, areas remote from divertor tiles, there is no direct loss of energetic triton, and charge exchanged tritium or thermalized tritium can be origins of remaining tritium in such area. On the other hand, tritium can migrate with carbon as tritiated hydrocarbon generated by chemical sputtering from divertor

tiles. That can be why amounts of remaining tritium are relatively large on material probes with carbon dominant deposition layer. In the case of C19-5 on which almost no deposition layer was formed, relatively large amount of remaining tritium was observed because the probe was located at the position where some of energetic triton lost [11]. In the case of C19-9O on which boron dominant deposition layer was formed, relatively large amount of tritium was also observed. It is speculated that absorption of tritium by boron layer caused the relatively large tritium retention.

## 7. CONCLUSION

As results various analyses of remaining tritium in divertor tiles and material probes located on the first wall, it was revealed that generated tritium during the first deuterium plasma experiment in LHD remained densely in divertor tiles and sparsely in the first wall. The largest amounts of remaining tritium among inner divertor tiles and material probes are approximately 0.3 GBq/m<sup>2</sup> and 0.6 MBq/m<sup>2</sup>, respectively. This distribution is strongly related to the distribution of lost points of energetic triton. The hydrogen plasma experiment conducted after the deuterium plasma experiment also affect the distribution of remaining tritium in divertor trace parts of inner divertor and outer divertor tiles. So far, the tritium particle balance has not been completely understood, and further analyses are necessary.

## ACKNOWLEDGEMENTS

The authors wish to thank the LHD experiment group for the excellent support of this work. S. M. is grateful for H. Yonezu, C. Iwata and D. Nagata for their dedicated technical support. S. M. is also grateful for Y. Suzuki for providing data related to lost points of high energy particles on plasma facing surfaces in LHD. This study was partially supported by a JSPS KAKENHI grant (18H01203).

## REFERENCES

- [1] H. Takahashi, et al., Nucl. Fusion **58** (2018), 106028.
- [2] K. Masaki, et al., J. Nucl. Mater. **313–316** (2003) 514.
- [3] C.W. Barnes, et al., Nucl. Fusion **38** (1998) 597.
- [4] H. Sjöstrand, et al., J. Phys. D: Appl. Phys. **41** (2008), 115208.
- [5] M. Yoshida, et al., Fus. Sci. Tech. **60** (2011) 1560.
- [6] T. Tanabe, Tritium: Fuel of Fusion Reactors, Springer, Berlin, 2017.
- [7] C. Stan-Sion, et al., Fus. Eng. Des. **89** (2014) 2628.
- [8] M. Isobe, et al., Nucl. Fusion **58** (2018) 082004.
- [9] M. Tanaka, et al., J. Nucl. Sci. Tech. **57** (2020) 1297.
- [10] S. Masuzaki, et al., Phys. Scr. **T171** (2020) 014068.
- [11] M. Yajima, et al., Nucl. Mater. Energy **27** (2021) 100906.
- [12] Y. Torikai, et al., Fusion Sci. Tech. **60** (2011) 1057.
- [13] G. Kikuchi et al., “Elucidation of location dependences of residual tritium measured by an autoclave method on first walls in LHD”, 29<sup>th</sup> Int. Toki Conf., Toki, Japan (2020)
- [14] Q. Zhou et al., Fus. Eng. Des. **159** (2020) 111879.
- [15] S. Masuzaki et al., Nucl. Mater. Energy **26** (2021) 100884.
- [16] K. Ogawa et al., Plasma Sci. Technol. **21** (2019) 025102.
- [17] S. Murakami et al., Trans. Fusion Technol. **27** (1995) 259.
- [18] V.K. Alimov et al., Fus. Eng. Des. **147** (2019) 111228.
- [19] G. Motojima et al., Nucl. Mater. Energy. **12** (2017) 1219.
- [20] M. Tanaka et al., J. Radioanal. Nucl. Chem. **318** (2018) 877.
- [21] C.N. Taylor, et al., AIP advances **7** (2017) 055305.
- [22] S.E. Lee et al., Annual reports of Hydrogen Isotope Research Center, U. Toyama, 38-1 (2018).
- [23] J. Allison, et al., Nucl. Instrum. Meth. Phys. Res. A, **835** (2016) 186.
- [24] J. Morimoto, et al., “Quantitative evaluation of wall heat loads by lost fast ions in the Large Helical Device”, 15<sup>th</sup> IAEA TCM on the Energetic Particles in Magnetic Confinement Systems, Princeton, USA (2017).
- [25] S. Masuzaki, et al., Nucl. Mater. Energy **18** (2019) 281.